Key Engineering Materials
ISSN: 1662-9795, Vol. 926, pp 970-979

Submitted: 2021-12-07
Revised: 2022-01-15
Accepted: 2022-02-04
Online: 2022-07-22

On the Anisotropic Mechanical Response of Ti6Al4V Sheet at High Strain Rates

Luca Corallo[1,a*] and Patricia Verleysen[1,b]

[1]Department of Electromechanical, Systems and Metal Engineering, MST-DyMaLab Research Group, Ghent University, Technologiepark 46, 9052 Zwijnaarde, Belgium

[a]Luca.Corallo@UGent.be, [b]Patricia.Verleysen@UGent.be

Keywords: Anisotropy, High strain rate, Ti6Al4V

Abstract. In traditional sheet metal forming processes, a thin sheet metal is deformed at relatively low speeds. However, more and more the speed of production processes is increased, very often to take advantage of the beneficial implications that high strain rates can have on the formability of certain metals. In this work, the effect of strain rate on the anisotropic behavior of Ti6Al4V is investigated performing tensile tests in different orientations, namely 0°, 45° and 90°, with respect to the rolling direction (RD), and in-plane shear experiments along RD. Three nominal strain rates, i.e., $8 \cdot 10^{-5}$, 0.5 and $1000 s^{-1}$, are considered. A novel high-speed bulge (HSB) test developed at Ghent University, designed to deform sheet metals in nearly equibiaxial loading conditions at high strain rates, is used for the dynamic bulge test. The experimental results, presented in this paper, clearly show the need of including the effect of strain rate, and eventually temperature, into the formulation of the yield function in order to correctly model and predict deformation processes performed at high speed.

Introduction

In traditional sheet metal forming processes, a thin sheet metal is deformed at relatively low speeds. However, more and more the speed of production processes is increased, very often to take advantage of the beneficial implications that high strain rates can have on the formability of certain metals. The design and optimization of high speed forming processes require in-depth knowledge of the sheet metal behavior under the conditions of strain and strain rate, met in high-speed forming processes. For this purpose, extensive test databases are needed. Tensile experiments at different orientations, with respect to the rolling direction, are commonly carried out to assess the material anisotropy in terms of yield strength and Lankford coefficient. Besides, experiments resulting in more complex stress states, i.e., shear, plane strain, biaxial, are performed to construct and validate the material yield surface [1]. Titanium alloys are widely used in several industrial sectors thanks to their excellent combination of mechanical strength and lightweight, and the good resistance to hostile environments, such as extreme temperatures and corrosive mediums. The anisotropic behavior of Ti6Al4V alloys has been investigated in-depth at room-temperature and at low strain rates [2–4]. A main feature reported by the studies is the tension-compression asymmetry, due to the activation of twinning when the plate material is deformed in compression. It has been reported that the tension-compression asymmetry highly affects the results of deep drawing operations in terms of thickness reduction, earing profile and drawing force [2]. In the last decades, modeling efforts have been directed to predict the peculiar yield locus of titanium [3–5]. However, most of these studies are limited to low strain rates. During high-speed forming operations, strain rate highly affects the forming properties of sheet metals [6], both in terms of material hardening and the related onset of strain localization [7]. In FE simulations, strain rate is taken into account in the constitutive material law. The strain rate sensitivity and adiabatic heating effect, i.e., the temperature rise due to the high-speed deformation, have been modelled for Ti6Al4V using the Johnson-Cook model [8]. The authors calibrated the model using tensile data obtained testing the material along the RD for a wide range of temperatures and strain rates. The anisotropic thermo-mechanical behavior of Ti6Al4V along RD and TD directions was also predicted using the KHL model [9]. In present work, the effect of strain rate on the anisotropic

behavior of Ti6Al4V is investigated performing tensile tests in different orientations, and in-plane shear experiments along RD. Three nominal strain rates, i.e., $8 \cdot 10^{-5}$, 0.5 and $1000s^{-1}$, are considered. The observed strain rate sensitivity and adiabatic heating effects are modeled using the Johnson-Cook constitutive law. Additionally, a dynamic bulge test is performed using the novel high-speed bulge (HSB) test developed at Ghent University [10]. The experimental results clearly show the need of including the effect of strain rate, and eventually temperature, on the formulation of the yield function in order to correctly model and predict deformation processes performed at high speed.

Material and Experimental Procedure

The investigated material is Ti6Al4V (ASTM Grade 5) provided by TIMET (Toronto, Canada) in the form of cold-rolled sheets obtained in mill-annealed condition with thickness of 0.6 ± 0.06mm. Table 1 shows the chemical composition reported by the manufacturer [11], as well as the limits defined in the AMS-4911 standard [12]. Ti6Al4V consists of a majority of hexagonal close packed α-phase and a finely dispersed body centered cubic β-phase. At room temperature approximately 4 vol% of β-phase is present. More details on the microstructure, including texture, can be found in [13].

Table 1: Chemical composition (% weight percent) of Ti6Al4V products reported by the supplier in the accompanying test reports [11]and defined in the ASM-4911standard [12].

		Fe	*V*	*Al*	*C*	*O*	*N*
TIMET		0.16	3.98	6.27	0.009	0.19	0.009
STANDARD	Min.	-	3.50	5.50	-	-	-
	Max.	0.30	4.50	6.75	0.080	0.20	0.050
Y,H and remaining elements : < 0.42. Remainder: Ti							

Tensile and in-plane shear samples are cut by means of electrical discharge machining (EDM). In *Fig. 1*, the technical drawings and nominal dimensions of the tensile and in-plane shear samples are presented.

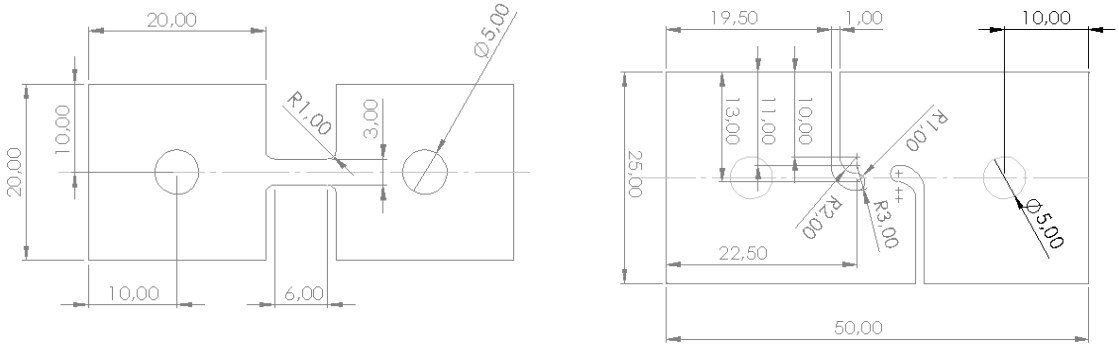

(a) (b)

Fig. 1: Geometry tensile (a) and in-plane shear (b) samples used for quasi-static and intermediate velocity experiments. Dimensions are given in mm.

The geometry of the tensile sample is optimized in order to avoid fracture at the sample shoulders and to achieve high strain rates during the dynamic testing. Tensile tests in different orientations, namely 0º, 45º and 90º, with respect to the rolling direction (RD), and in-plane shear experiments along RD are performed. The effect of strain rate on the material anisotropic response is investigated for three different nominal strain rates, i.e., $8 \cdot 10^{-5}$, 0.5 and $1000s^{-1}$. Quasi-static and intermediate experiments are performed using an Instron 5569 device equipped with a 50kN loadcell, while dynamic experiments are carried out using a split Hopkinson tensile bar. For quasi-static and intermediate strain rate experiments, the samples are connected to the Instron by means of pins inserted between the sample (see Fig. 1) and the machine grabs. For the dynamic tests, the sheet samples are glued in slots made in the Hopkinson bars in order to guarantee quasi-static equilibrium

from the early stage of loading and avoid oscillations in the wave measurements leading at possible inaccuracies in the determination of the material yielding. For this purpose, the width of the clamping region of the sample is increased from 20mm to 25mm, i.e., the diameter of the Hopkinson bars. Before an experiment, a stochastic white/black speckle pattern is applied to the sample surface. During the test, the sample surface is continuously recorded using a camera placed in front of the sample surface. The camera used for the quasi-static experiments is a 5Mpxls Allied Vision Stingray F-504, while a Photron mini AX200 is employed for both intermediate and dynamic tests. Frame rates of $6 \cdot 10^{-2}$, 500 and $120 \cdot 10^{3}$ fps are used for the quasi-static, intermediate and dynamic experiments, respectively. The experimental setups used for the tensile and shear experiments are shown in Fig. 2.

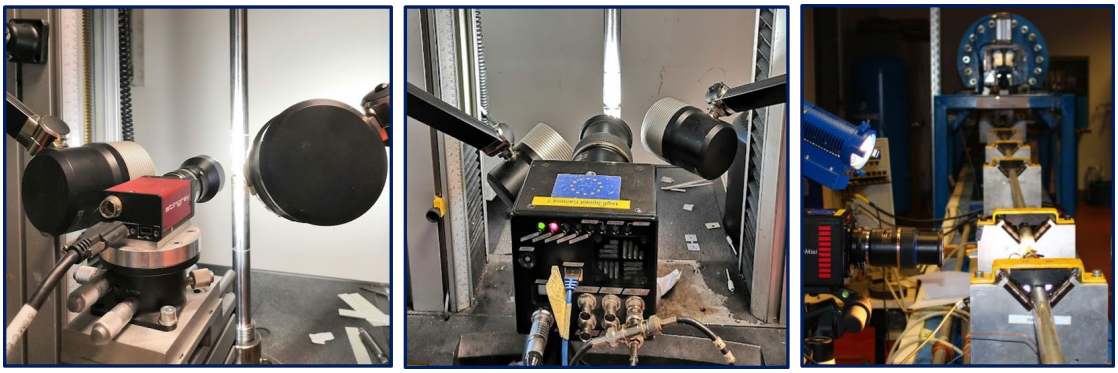

(a) (b) (c)

Fig. 2: Experimental setups used for tensile and in-plane shear experiments at low (a), intermediate (b) and high strain rates (c).

A dynamic nearly equibiaxial experiment on a circular sample is performed using the high-speed bulge (HSB) setup shown in Fig. 3(a). The HSB setup combines features of both split Hopkinson pressure bar (SHPB) and hydraulic bulge tests. The special configuration of the bars leaves the sample surface accessible for full-field displacement and strain mapping. The Hopkinson input bar is in contact with a piston, inserted into a hydraulic chamber realized inside the hollow output bar tube. A schematic representation of the hydraulic chamber is shown in Fig. 3(b).

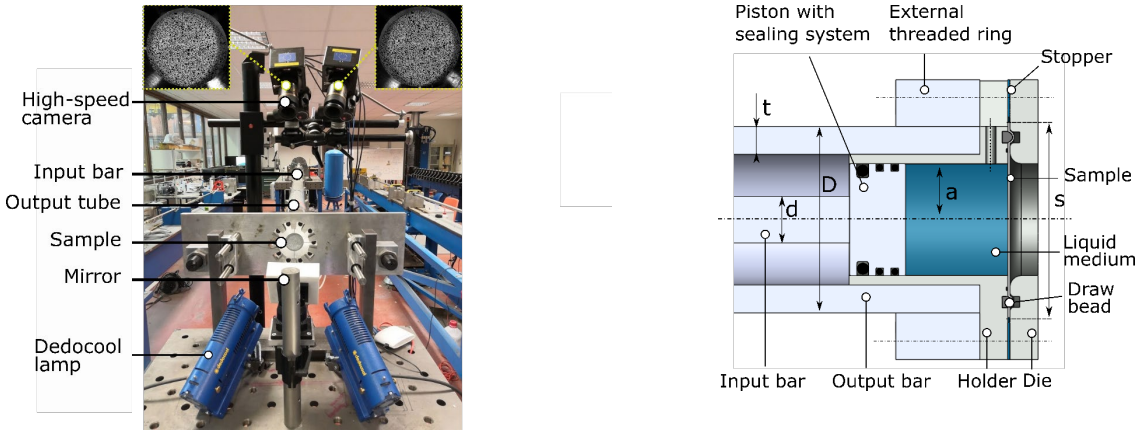

(a) (b)

Fig. 3 High speed bulge setup installed at DyMaLab of Ghent University (a) and schematic representation of the components of the hydraulic chamber (b). The dimensions are the following: d=25mm, D=100mm, t=15mm, a=30mm and s=52mm.

For the HSB experiment, optical measurements at the sample surface are carried out using two high-speed Photron mini AX200 cameras positioned under an angle to allow stereo imaging with an acquisition rate of $36 \cdot 10^{3}$ fps. More information regarding the HSB setup can be found in [10]. From the recorded images, the strain fields and 3D displacements at the sample surface are measured using the DIC commercial software provided by MatchID. The impact of the projectile at the free end

of the input bar generates a compressive wave traveling in the input bar towards the hydraulic piston. The piston subsequently pressurizes the liquid in the hydraulic chamber and thus deforms the sample. The dynamic load needed to deform the sample is transferred to the output tube as a tensile wave with strain amplitude ε_t. In the input bar, a reflected tensile wave is observed. Eq. (1) is used to derive the pressure acting at the sample surface:

$$p(t) = \frac{A_{out}E_{out}}{\pi a^2}\varepsilon_t(t) \tag{1}$$

E_{out} and A_{out} are the elastic modulus and section of the output bar, respectively, and a is the hydraulic chamber radius. The material hardening is calculated based on a theory proposed by [14] and the procedure described in the standard ISO 16808:2014. Eqs. (2) and (3) are used to compute the equivalent strain and the von Mises stress at the sample apex respectively.

$$\varepsilon = ln\left(\frac{t}{t_0}\right) \tag{2}$$

Where t_0 is the initial sample thickness, and t is the actual thickness at the sample apex derived from the in-plane components of the strain assuming volume conservation.

$$\sigma = \frac{pR}{2t} \tag{3}$$

Where R is the radius of the deformed sample at the apex and p is the hydraulic pressure acting at the sample surface. A 2th order polynomial function is used for the determination of the principal curvatures in the rolling and transverse direction i.e., k_{RD} and k_{TD}. The average curvature radius is calculated as $R = 2/(k_{RD} + k_{TD})$. The fitting procedure is performed for every image, i.e., time step, and for all the data points located within $\pm 20\ mm$ with respect to the sample apex. A HBM transient recorder with acquisition rate of 1MHz is used to measure the incident loading, reflected and transmitted waves from strain gauges attached to the Hopkinson bars during the experiments.

Results

Tensile tests

For the quasi-static and intermediate velocity experiments, the tensile force is measured from the Instron loadcell. In the dynamic experiments, the tensile force is determine from the transmitted wave ε_t traveling in the output bar, using the one-dimensional wave propagation theory [15]: $F = A_b E_b \varepsilon_t$. Where E_b and A_b are the Young's modulus and the section of the out bar respectively. The true strain along the loading direction is measured by means of DIC, while the true stress is calculated as $\sigma_t = F/A_s$, where A_s is the section of the sample in the diffuse necking region. The thickness reduction is calculated using the hypothesis of volume conservation. The true curves are reported Fig. 4 up to a true plastic strain of 10%. The average of the diffuse necking for the three directions is indicated by a vertical dashed line. DIC is used to determine the Lankford coefficients (r-values), defined as the ratio between the in-plane width and through-thickness plastic strain increments, $r = \dot{\varepsilon}_w^p/\dot{\varepsilon}_t^p = -\dot{\varepsilon}_w^p/(\dot{\varepsilon}_l^p + \dot{\varepsilon}_w^p)$. Where the subscripts w, t and l are used to indicate the width, thickness and longitudinal sample directions. The thickness strain is calculated assuming volume conservation. The longitudinal and width plastic strains, i.e., ε_l^p and ε_w^p , evolve almost linearly with time, hence for any given test, the Lankford can be considered constant. The presented r-values are averaged from onset of yielding till the onset of diffuse necking.

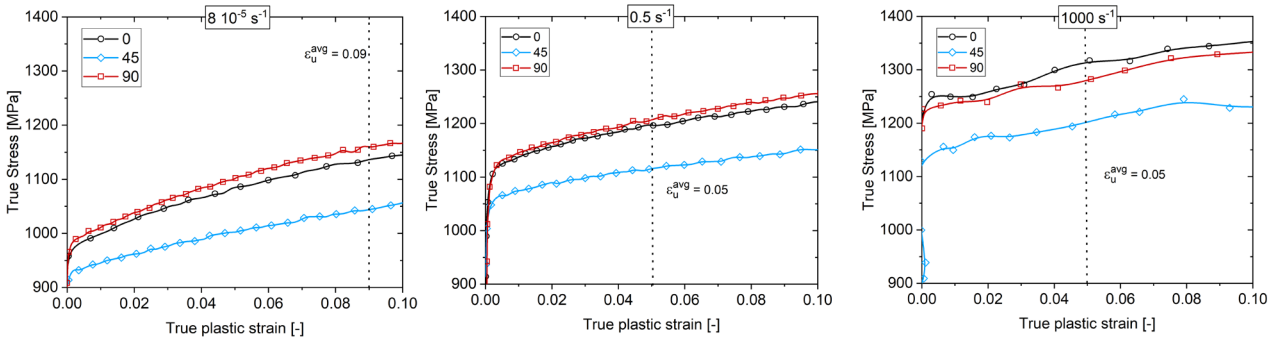

(a) (b) (c)

Fig. 4: True stress strain curves tensile experiments at 0º, 45º and 90º with respect to RD at low (a), intermediate (b) and high (c) strain rates ($8 \cdot 10^{-5}$, 0.5 and $1000s^{-1}$).

In Fig. 5 the normalized uniaxial yield stresses (σ_θ/σ_0) at 1% of plastic strain, and the r-values, are plotted with respect to the angle θ between the loading direction and RD, for the considered three different nominal strain rates. The values of normalized stress and r-values shown in Fig. 5 are compiled in Table 2.

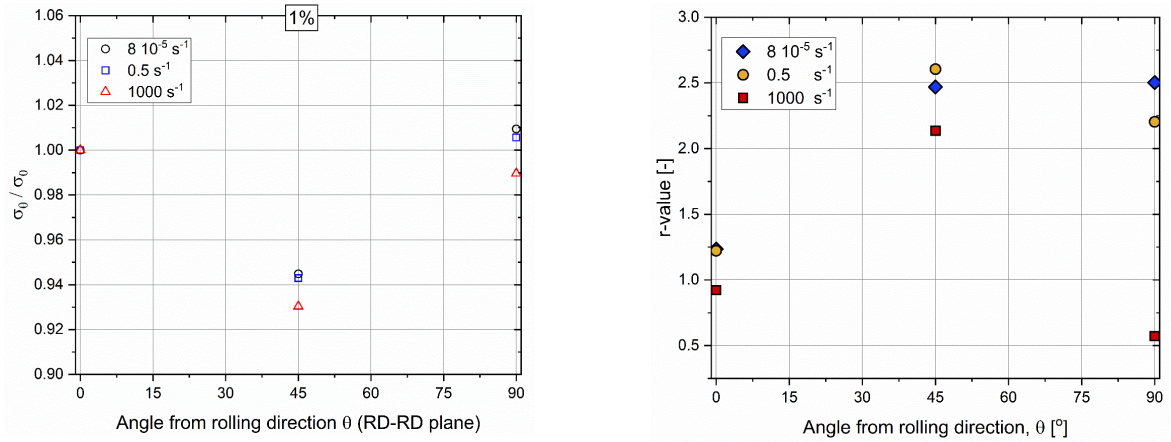

(a) (b)

Fig. 5: Normalized stress versus angle from rolling direction at 1% of plastic strain (a) and r-values versus angle from rolling direction (b) for three different nominal strain rates ($8 \cdot 10^{-5}$, 0.5 and $1000s^{-1}$).

Table 2: Normalized stress at 1% of plastic strain and r-values, for three different nominal strain rates ($8 \cdot 10^{-5}$, 0.5 and $1000s^{-1}$).

	0º			*45º*			*90º*		
Nominal $\dot{\varepsilon}$ $[s^{-1}]$	*8 10-5*	*0.5*	*1000*	*8 10-5*	*0.5*	*1000*	*8 10-5*	*0.5*	*1000*
r-values	1.23	1.22	0.92	2.47	2.60	2.14	2.50	2.20	0.57
σ_θ/σ_0	1	1	1	0.945	0.943	0.930	1.009	1.006	0.989

Thermal softening and strain rate sensitivity

When experiments are performed at intermediate and high strain rates, during the plastic deformation, a significant part of the plastic work is converted into heat which is not dissipated to the environment, resulting in a local increment of the sample temperature, and thus, in thermal softening. Starting from an initial temperature T_0, the local temperature increment, as a function of the plastic strain ε_p, can be calculated through the integral of the plastic work:

$$T(\varepsilon_p) = T_0 + \frac{\beta}{\rho C}\int_0^{\varepsilon_p} \sigma d\varepsilon_p \quad (4)$$

Where ρ is the density of the material, C is the specific heat, and β is the so called Taylor–Quinney coefficient expressing the fraction of the plastic work transformed into heat. Besides the adiabatic heating, the strain rate itself can have a, generally positive, effect on the material hardening. The strain rate sensitivity and thermal softening are often modelled using the Johnson-Cook (JC) hardening model:

$$\sigma(\varepsilon_p, \dot{\varepsilon}, T) = \sigma_0(\varepsilon_p) \cdot \mathrm{k_{SR}}(\dot{\varepsilon}) \cdot \mathrm{k_T(T)} = \left(\mathrm{A} + \mathrm{B}\varepsilon_p^n\right)\left(1 + \mathrm{C}\ln\frac{\dot{\varepsilon}}{\dot{\varepsilon}_0}\right)\left[1 - \left(\frac{\mathrm{T} - \mathrm{T_r}}{\mathrm{T_m} - \mathrm{T_r}}\right)^{\mathrm{m}}\right] \quad (5)$$

In eq. *(5)*, the strain rate hardening and thermal softening are taken into account by multiplying the reference stress $\sigma_0(\varepsilon_p)$, at the reference strain rate $\dot{\varepsilon}_0$ and temperature T_r, by a strain rate sensitivity factor $k_{SR}(\dot{\varepsilon})$, and temperature sensitivity $k_T(T)$ factor. The material parameters of the JC hardening model and the Taylor–Quinney coefficient for the Ti6Al4V were determined for the RD in [8] and reported in Table 3.

Table 3: Parameters JC hardening model and Taylor–Quinney coefficient for Ti6Al4V *[8]*.

A [MPa]	*B [MPa]*	*n*	*C*	*m*	*β*
2.756 10^6	1.657 10^6	0.48	0.0138	1.79 10^{-4}	0.46

It has to be mentioned that the best fit for the JC parameters was found fitting the experimental curves considering the absolute zero (0K or -273°C) as reference temperature, and the strain rate $8 \cdot 10^{-5} s^{-1}$ as reference strain rate. Moreover, [8] demonstrated that for $\dot{\varepsilon} \geq 0.5\ s^{-1}$ the experiments are fully adiabatic. The temperature sensitivity $k_T(T)$ can be used to convert any material hardening curve obtained in adiabatic conditions to the respective isothermal curve at room temperature, i.e., $\sigma_{cooled-down}(\varepsilon_p, \dot{\varepsilon}, T_r) = \sigma(\varepsilon_p, \dot{\varepsilon}, T_{exp})\frac{k_T(T_r)}{k_T(T_{exp})}$. This procedure is further indicated as *cooled-down*. Likewise, the strain rate sensitivity $k_{SR}(\dot{\varepsilon})$ can be used to eliminate the effect of strain rate from the intermediate and high strain rate experiments, i.e., $\sigma_{slowed-down}(\varepsilon_p, \dot{\varepsilon}_0, T) = \sigma(\varepsilon_p, \dot{\varepsilon}_{exp}, T)\frac{1}{k_{SR}(\dot{\varepsilon}_{exp})}$. This procedure is further indicated as *slowed-down*. The two procedures, *cooled-down* and *slowed-down*, are employed to verify if strain rate and thermal softening factors assessed for the RD are also valid for the tensile data obtained at different orientations, namely if there is any dependency between strain rate, temperature and material anisotropy. More details regarding the procedure to obtain the isothermal curve at the reference strain rate can be found in [16]. In Fig. 6, the experimental hardening curves, and the respective cooled-down and slowed-down curves, are presented.

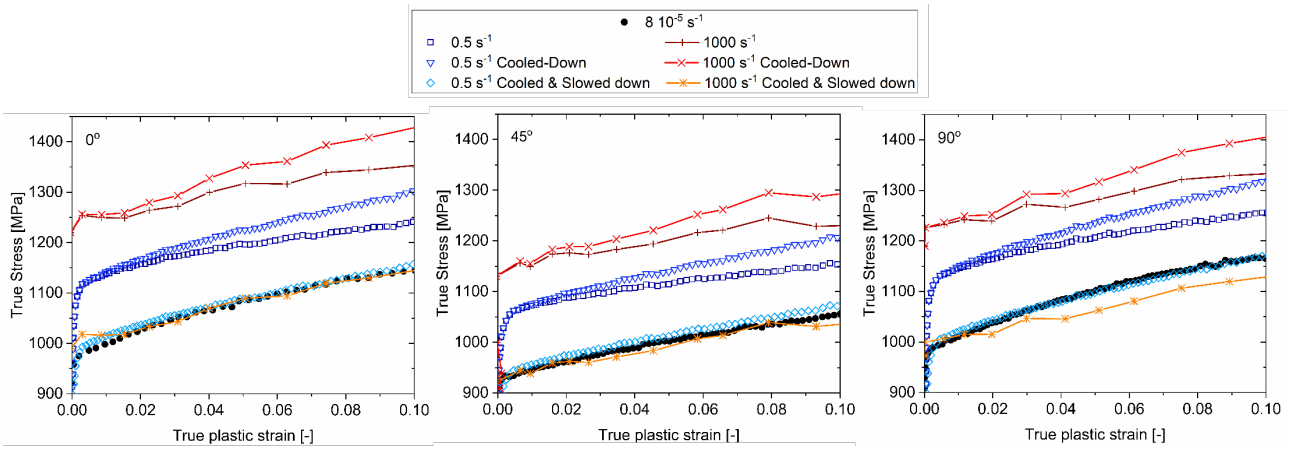

Fig. 6: Experimental hardening curves, and cooled-down and slowed-down curves obtained for intermediate and high strain rates experiments, for three different orientations (0°, 45° and 90° with respect to RD).

In-plane shear

The optimized in-plane shear sample geometry allows to characterise the static and dynamic shear behaviour of sheet metals employing the same tensile test devices used for tensile experiments [17]. The true shear stress is derived following the same procedure described for the tensile experiment, while the logarithmic shear strain is assessed by means of 2D DIC measurements at the sample surface. The strain is measured in the homogeneous blue region in Fig. 7, which shows the contour plot of the logarithmic shear strain for the low speed experiment before failure. The shear stress versus true logarithmic shear strain is reported in Fig. 8 for the three considered strain rates.

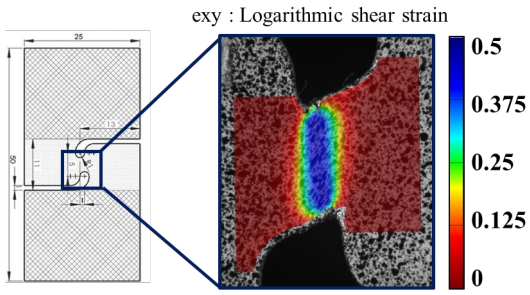

Fig. 7: Contour plot logarithmic shear strain experiment at low speed. Frame before fracture.

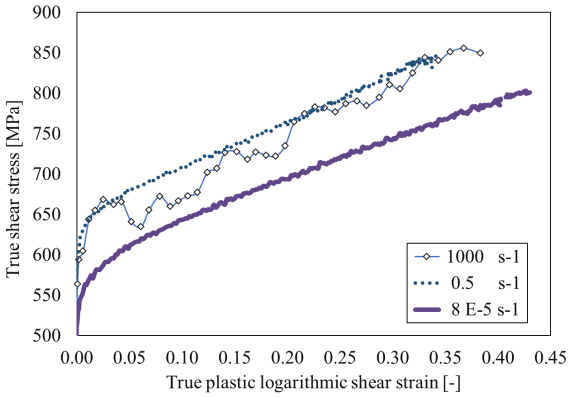

Fig. 8: True shear stress versus true plastic logarithmic shear strain for three different nominal strain rates.

High speed bulge experiments

The high speed bulge test is performed for a nominal strain rate of $150s^{-1}$. The bulge stress, corresponding with the von Mises stress, together with the evolution of the strain rate at the sample apex is plotted in Fig. 9 with respect to the plastic strain. The strain rate is calculated as time derivative of the through thickness strain given by eq. (2). The sample is plastically deformed till a level of plastic deformation of 14%. The deformation level achieved during the test is related to the incident and transmitted wave amplitudes and loading duration. Larger strain levels, till fracture, can be achieved for higher amplitudes of the incident wave.

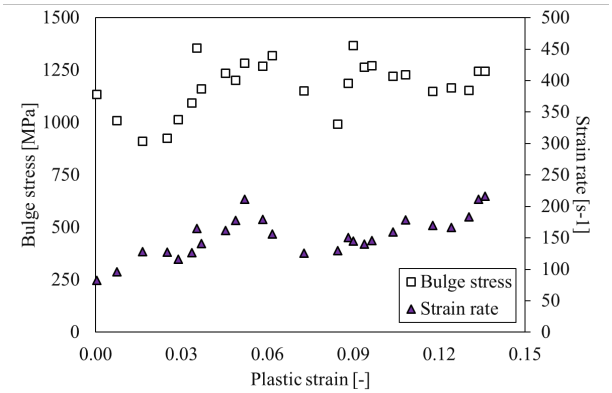

Fig. 9: Bulge stress and strain rate at the sample apex with respect to the plastic strain.

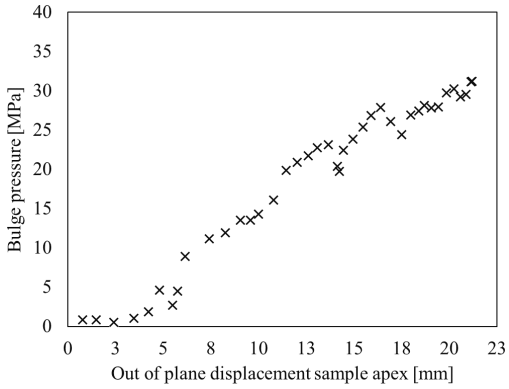

Fig. 10: Bulge pressure versus the out of plane displacement at the sample apex.

Noticeable oscillations are observed in the stress level. Indeed, during the HSB test, the sample is accelerated by a dynamic load, resulting in the vibration of the sample. The ringing of the sample is reflected in the radius of curvature, and thus in the bulge stress [10]. Nevertheless, Fig. 9 gives a valuable insight into the effect of a high strain rate on the mechanical behaviour of the tested material under nearly equibiaxial stress state. Moreover, the HSB gives access to macroscopic results, such as bulge pressure, displacement and strain fields at the sample surface. In Fig. 10 the evolution of the bulge pressure is plotted as a function of the out of plane displacement at the sample apex measured

using the stereo DIC technique. Contour plots of the out of plane displacements at different instants of the experiment are reported in Fig. 11.

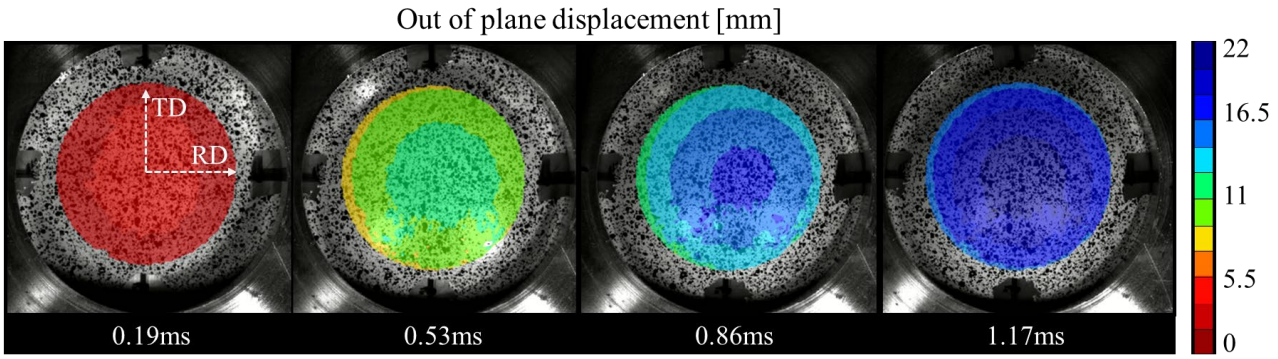

Fig. 11: Contour plots out of plane displacements at four different instants of the HSB experiment.

Discussion

The results of the tensile experiments, i.e., normalized stresses and r-values, at quasi-static loading conditions are in agreement with the data reported in [3]. The strain rate has the same effect on the material yielding for all the tensile experiments, indeed the trend of the normalized stress is almost the same for all the orientations irrespective of the deformation speed, see Fig. 5a. On the other hand, Fig. 5b shows that the r-value drastically decreases with increasing strain rate when the material is tested along the TD. The results of the tensile tests clearly indicate the need to include the effect of strain rate, and also temperature, into the formulation of the yield function in order to correctly model and predict deformation processes performed at high speed. Concerning the material hardening, the JC constitutive model as calibrated in [8] for the RD, is able to account for both the strain rate sensitivity and adiabatic temperature rise, for the RD and 45° experiments. Indeed, the hardening curves obtained for the intermediate and high strain rate experiments, corrected using JC for the adiabatic heating effects (cooled-down) and strain rate (slowed-down), completely overlap with the quasi-static reference curves, from onset of yielding till 10% of plastic strain, see Fig. 6. However, the correction procedure becomes less accurate when it is used for the experiments performed in the TD. Additional experiments, in more directions, would be required to verify the validity of the correction procedure, and thus, the use of the JC constitutive model calibrated only based on results obtained for the RD. The shear experiment allows to identify the material hardening for larger levels of plastic strain, compared to the tensile tests, since no necking occurs during the experiment. In contrast to what is observed for the tensile experiments, where an increasing strain rate results in higher stress levels, in the shear experiments, intermediate and high strain rate experiments result in a similar stress amplitude, see Fig. 8. The shear experiments suggest the existence of a relationship between the stress state and strain rate sensitivity. The HSB experiment provides new insights on the elastoplastic deformation of Ti6Al4V under a nearly equibiaxial stress state at high strain rates. The hardening curve, obtained for a nominal strain rate of $150s^{-1}$, can be used for the calibration of anisotropic, strain rate dependent yield functions. However, as reported by [18], the correct quantification of the bulge stress would require the knowledge of the yield criterion describing the anisotropic behaviour of the material. On the other hand, global experimental data from the HSB test, such as pressure evolution, displacement and strain fields at the sample surface, can be used for the validation of strain rate dependent, anisotropic models. Indeed, the extensive dataset available from HSB experiments can be employed for inverse, combined numerical-experimental identification techniques, such as the ones presented in [19,20].

Conclusions

The effect of strain rate on the anisotropic behaviour of Ti6Al4V is investigated performing tensile tests in different orientations, namely 0º, 45º and 90º, with respect to the rolling direction (RD), and in-plane shear experiments along RD. Three nominal strain rates, i.e., $8 \cdot 10^{-5}$, 0.5 and $1000 s^{-1}$, are considered. A novel high-speed bulge (HSB) test developed at Ghent University [10], designed to deform sheet metals in nearly equibiaxial loading conditions and high strain rates, is used for the dynamic bulge test. The tensile results reveal the influence of strain rate on the Lankford coefficient for the experiment along TD, namely a reduction of about 75% with respect to the quasi-static condition, while no variations on the normalized stress were observed. The Johnson-Cook hardening model, calibrated along the RD in [8], has been successfully used to account for the strain rate sensitivity and adiabatic temperature rise for the experiments at 0º and 45º. However, the JC model becomes less accurate when employed for the experiment at 90º. In the shear experiments, a saturation of the strain rate sensitivity for the high strain rate experiment is observed. The HSB test allows to extract the material hardening under nearly equibiaxial loading condition, and a strain rate of about $150 s^{-1}$, up to a plastic strain of about 14%. The experimental data available from the HSB test can be used for the calibration of anisotropic, strain rate dependent models, as well as for validation purposes. Indeed, the large dataset available from the HSB, such as pressure evolution, displacement and strain fields, can be employed for inverse, combined numerical-experimental identification techniques, such as these presented in [19,20]. The experimental results presented in this paper clearly indicate the need of including the effect of strain rate, and eventually temperature, on the formulation of the yield function in order to correctly model and predict deformation processes performed at high speed. Moreover, the shear experiments suggest the existence of a relationship between stress state and strain rate sensitivity. Future work is oriented towards using the presented dataset, i.e. tensile and shear results, to calibrate strain rate dependent, anisotropic models. Additionally, the HSB results will be used to validate the calibrated model.

References

[1] Badr OM, Barlat F, Rolfe B, Lee M-G, Hodgson P, Weiss M. Constitutive modelling of high strength titanium alloy Ti-6Al-4 V for sheet forming applications at room temperature. International Journal of Solids and Structures 2016;80:334–47.

[2] Lin P, Hao YG, Zhang BY, Chi CZ, Cui XL, Shen J, et al. Planar Anisotropy, Tension–Compression Asymmetry, and Deep Drawing Behavior of Commercially Pure Titanium at Room Temperature. J of Materi Eng and Perform 2019;28:1734–44.

[3] Gilles G, Hammami W, Libertiaux V, Cazacu O, Yoon JH, Kuwabara T, et al. Experimental characterization and elasto-plastic modeling of the quasi-static mechanical response of TA-6V at room temperature. International Journal of Solids and Structures 2011;48:1277–89.

[4] Tuninetti V, Gilles G, Milis O, Pardoen T, Habraken AM. Anisotropy and tension–compression asymmetry modeling of the room temperature plastic response of Ti–6Al–4V. International Journal of Plasticity 2015;67:53–68.

[5] Nixon ME, Cazacu O, Lebensohn RA. Anisotropic response of high-purity α-titanium: Experimental characterization and constitutive modeling. International Journal of Plasticity 2010;26:516–32.

[6] Verleysen P, Peirs J, Van Slycken J, Faes K, Duchene L. Effect of strain rate on the forming behaviour of sheet metals. Journal of Materials Processing Technology 2011;211:1457–64.

[7] N'souglo KE, Rodríguez-Martínez JA, Vaz-Romero A, Cazacu O. The combined effect of plastic orthotropy and tension-compression asymmetry on the development of necking instabilities in flat tensile specimens subjected to dynamic loading. International Journal of Solids and Structures 2019;159:272–88.

[8] Galán J, Verleysen P, Degrieck J. Thermal Effects During Tensile Deformation of Ti-6Al-4V at Different Strain Rates: Thermal Effects During Deformation of Ti-6Al-4V at Different Strain Rates. Strain 2013;49:354–65.

[9] Khan AS, Yu S. Deformation induced anisotropic responses of Ti–6Al–4V alloy. Part I: Experiments. International Journal of Plasticity 2012;38:1–13.

[10] Corallo L, Verleysen P. The split Hopkinson bar bulge setup: a novel dynamic biaxial test method. EPJ Web Conf 2021;250:01019. https://doi.org/10.1051/epjconf/202125001019.

[11] Certificate of conformity. H9421-01. Canada:Timet; 2002. n.d.

[12] SAE International. AMS-4911M: titanium alloy, sheet, strip and plate, 6AL-4V, annealed. 1977. n.d.

[13] Galán-López J, Verleysen P. Simulation of the plastic response of Ti–6Al–4V thin sheet under different loading conditions using the viscoplastic self-consistent model. Materials Science and Engineering: A 2018;712:1–11.

[14] Hill R. C. A theory of the plastic bulging of a metal diaphragm by lateral pressure. The London, Edinburgh, and Dublin Philosophical Magazine and Journal of Science 1950;41:1133–42.

[15] Graff KF. Wave Motion in Elastic Solids. Courier Corporation; 2012.

[16] Jesus Galan Lopez. Crystal Plasticity Based Modelling of the Strain Rate Dependent Mechanical Behaviour of Ti6Al4V. (Doctoral dissertation). Ghent University, 2013.

[17] Peirs J, Verleysen P, Degrieck J. Novel Technique for Static and Dynamic Shear Testing of Ti6Al4V Sheet. Experimental Mechanics 2012;52:729–41.

[18] Cazacu O, Revil-Baudard B. Forming of titanium materials. Plasticity of Metallic Materials, Elsevier; 2021, p. 479–537.

[19] Avril S, Bonnet M, Bretelle A-S, Grédiac M, Hild F, Ienny P, et al. Overview of Identification Methods of Mechanical Parameters Based on Full-field Measurements. Exp Mech 2008;48:381–402.

[20] Coppieters S, Kuwabara T. Identification of Post-Necking Hardening Phenomena in Ductile Sheet Metal. Exp Mech 2014;54:1355–71.